

## Supporting information

### **A novel NIR fluorescent probe for *in situ* visualizing of Fe(II) and its application in drug-induced liver/kidney injury**

Hanyue Xiang <sup>a</sup>, Yanjie Song <sup>a</sup>, Yilin Wang <sup>b</sup>, Wenzhuo Fu <sup>c</sup>, Nao Xiao <sup>a,\*</sup>

<sup>a</sup> Beijing Area Major Laboratory of Peptide and Small Molecular Drugs, Engineering Research Center of Endogenous Prophylactic of Ministry of Education of China, School of Pharmaceutical Sciences, Capital Medical University, Beijing, 100069, China

<sup>b</sup> School of Basic Medical Sciences, Capital Medical University, Beijing 100069, China

<sup>c</sup> Core Facilities Center, Capital Medical University, Beijing 100069, China

\* Corresponding author.

E-mail address: xiaonao@ccmu.edu.cn (N. Xiao).

### Table of Contents:

Page	Description	Comment
1-7	Experimental section.	
8	Main fluorescent probe types for Fe <sup>2+</sup> .	Scheme S1
8	<sup>1</sup> H NMR spectrum of <b>1</b> in DMSO- <i>d</i> <sub>6</sub> .	Figure S1
9	<sup>13</sup> C NMR spectrum of <b>1</b> in DMSO- <i>d</i> <sub>6</sub> .	Figure S2
9	ESI-MS spectrum of <b>1</b> .	Figure S3
10	<sup>1</sup> H NMR spectrum of <b>MDJ</b> in CDCl <sub>3</sub> .	Figure S4
10	<sup>13</sup> C NMR spectrum of <b>MDJ</b> in CDCl <sub>3</sub> .	Figure S5
11	ESI-MS spectrum of <b>MDJ</b> .	Figure S6
12	X-ray crystal structure of <b>MDJ</b> .	Figure S7
13	<sup>1</sup> H NMR spectrum of <b>MDJ-O</b> in CDCl <sub>3</sub> .	Figure S8
13	<sup>13</sup> C NMR spectrum of <b>MDJ-O</b> in CDCl <sub>3</sub> .	Figure S9
14	ESI-MS spectrum of <b>MDJ-O</b> .	Figure S10
15	ESI-MS spectrum of <b>MDJ-O</b> in the presence of Fe <sup>2+</sup> .	Figure S11
15-16	Fluorescence spectra of <b>MDJ-O</b> towards Fe <sup>2+</sup> in various solvents.	Figure S12-S14
17	Fluorescence emission intensities of <b>MDJ-O</b> response to Fe <sup>2+</sup> .	Figure S15
17	The size distribution analysis of <b>MDJ-O</b> and <b>MDJ-O</b> + Fe <sup>2+</sup> .	Figure S16
18	Fluorescence excitation and emission spectra of <b>MDJ</b> , <b>MDJ-O</b> and <b>MDJ-O</b> after the reaction with Fe <sup>2+</sup> .	Figure S17-S18
19	Time–trace plots of <b>MDJ-O</b> towards Fe <sup>2+</sup> .	Figure S19
20	The limit of detection (LOD) of <b>MDJ-O</b> towards Fe <sup>2+</sup> .	Figure S20
21	Fluorescent spectral changes of <b>MDJ-O</b> upon addition various analytes.	Figure S21-22
22	Cytotoxicity study in HepG2 cells.	Figure S23
22	Mean fluorescence intensities of confocal image Figure 4B.	Figure S24
23	The photostability of <b>MDJ-O</b> in living cells.	Figure S25
24-25	Co-localization imaging in HepG2 cells.	Figure S26-S27
25	Fluorescence images of zebrafish.	Figure S28
26	Images of the liver and kidney.	Figure S29
26	H&E-staining of internal organs sections.	Figure S30-S31
27	Crystal data and structure refinement for <b>MDJ</b> .	Table S1
28	Bond lengths [Å] of <b>MDJ</b> crystal.	Table S2
29	Bond angles [°] for <b>MDJ</b> crystal.	Table S3
30-33	Examples of various Fe <sup>2+</sup> probes.	Table S4
34-35	References	

## Apparatus

<sup>1</sup>H NMR and <sup>13</sup>C NMR spectra data were acquired on a Bruker AVANCE II 300 MHz spectrometer. DMSO-*d*<sub>6</sub> and CDCl<sub>3</sub> were used as solvents and chemical shifts were recorded using tetramethylsilane (TMS,  $\delta = 0$  ppm) as the internal standard. UV–visible absorption spectra were recorded using a UV-2600 UV–vis ultraviolet spectrophotometer (Shimadzu, Japan) in 1.0-cm-path-length cuvette. Emission spectra were measured on an RF-6000 spectrometer (Shimadzu, Japan) at room temperature. The pH values were measured by a PHS-3C digital pH meter (Shanghai INESA Scientific Instrument Co., Ltd., China). Diverse pH values were adjusted by NaOH or HCl solution. A Quattro Micro tandem quadrupole mass spectrometry (Waters, USA) with accessories (ESI source-atmospheric pressure electrospray ion source) was used for mass spectrometry analyses. The source conditions of pressure, dry temp, and resolution ratio were set as 30 V, 105 °C, and 0.4 amul respectively. The chromatography coordinates were taken by an Edinburgh Instruments of FLS980 spectrometer. HPLC was performed on HPLC-1675 (Aligent, USA). The absorbance of MTT was measured by the Enspire multifunctional microplate Reader (PerkinElmer, USA). Fluorescence intensity data of cells were obtained by LSR Fortessa flow cytometer (BD, USA). Sample detection speed:  $\geq 70000$  cells/s. The detection dead time was 0. The excitation wavelength was 561 nm. Cell imaging was performed by a TCS SP8 STED super-resolution confocal microscope (Leica, Germany). All animal images were acquired by IVIS Spectrum *in vivo* imaging System (PerkinElmer, USA).

## Materials

Isophorone, malononitrile, and hexadecyl trimethyl ammonium bromide (CTAB) were purchased from Beijing InnoChem Science and Technology Co., Ltd. 2,3,6,7-Tetrahydro-1H,5H-benzo[*ij*]quinolizine-9-carboxaldehyde were purchased from Shanghai Bide Pharmatech Co., Ltd. 3-Chloroperoxybenzoic acid (*m*-CPBA), acetaminophen (APAP), and dimethylamine were purchased from Shanghai Macklin Biochemical Co., Ltd. The common solvents such as ethanol (EtOH), ethyl acetate (EtOAc), methanol (MeOH), tetrahydrofuran (THF), dimethylformamide (DMF), dimethyl sulfoxide (DMSO) and phosphate buffer saline (PBS, 10 mM, pH=7.4) were purchased from Beijing Chemical Works Co., Ltd. The metal salts for providing metal ions are lithium chloride (LiCl), sodium sulfate (Na<sub>2</sub>SO<sub>4</sub>), magnesium sulfate (MgSO<sub>4</sub>), potassium nitrate

(KNO<sub>3</sub>), calcium chloride (CaCl<sub>2</sub>), chromium(III) chloride hexahydrate (CrCl<sub>3</sub>·6H<sub>2</sub>O), ferrous sulfate heptahydrate (FeSO<sub>4</sub>·7H<sub>2</sub>O), cobalt(II) chloride hexahydrate (CoCl<sub>2</sub>·6H<sub>2</sub>O), nickel(II) chloride(NiCl<sub>2</sub>), copper sulfate pentahydrate (CuSO<sub>4</sub>·5H<sub>2</sub>O), zinc perchlorate (Zn(ClO<sub>4</sub>)<sub>2</sub>·6H<sub>2</sub>O), cadmium chloride (CdCl<sub>2</sub>) and were purchased from Shanghai Macklin Biochemical Co., Ltd. The anions were gained from their sodium, potassium, or tetrabutylammonium salts including tetrabutylammonium iodide (TBAI, I<sup>-</sup>), tetrabutylammonium bromide (TBABr, Br<sup>-</sup>), tetrabutylammonium chloride (TBACl, Cl<sup>-</sup>), potassium sulfide (K<sub>2</sub>S, S<sup>2-</sup>), sodium pyrophosphate decahydrate (Na<sub>4</sub>P<sub>2</sub>O<sub>7</sub>·7H<sub>2</sub>O, PPI), tetrabutylammonium cyanide (TBACN, CN<sup>-</sup>), potassium nitrate (KNO<sub>3</sub>, NO<sub>3</sub><sup>-</sup>), zinc perchlorate (Zn(ClO<sub>4</sub>)<sub>2</sub>, ClO<sub>4</sub><sup>-</sup>), sodium bicarbonate (NaHCO<sub>3</sub>, HCO<sub>3</sub><sup>-</sup>), and nickel(II) acetate tetrahydrate (Ni(CH<sub>3</sub>CO<sub>2</sub>)<sub>2</sub>, CH<sub>3</sub>CO<sub>2</sub><sup>-</sup>). The other analytes including cysteine (Cys), homocysteine (Hcy), glutathione (GSH), glycine (Gly), lysine (Lys), arginine (Arg), adenosine triphosphate (ATP), vitamin C (Vit-C) were purchased from Shanghai Macklin Biochemical Co., Ltd. All solvents and chemical reagents were used as received without further purification. The deionized water used in all experiments was Wahaha water (Hangzhou wahaha group Co. Ltd. China). Dulbecco's modified eagle medium (DMEM), penicillin-streptomycin liquid, fetal bovine serum (FBS), trypsin solution were purchased from America Thermo Fisher Scientific Co., Ltd. Human hepatocellular carcinoma (HepG2) cells used in this study were purchased from Wuhan Procell Life Science and Technology Co., Ltd. Adult zebrafish were purchased from Nanjing Eze-Rinka Co., Ltd. The male Kunming mice (20 ± 2 g) were purchased from Beijing Vital River Laboratory Animal Technology Co., Ltd. The animal experimental protocols have passed the ethical review, and all animal care and experimental protocols were complied with the ethical principles.

### **Crystal characterization**

**MDJ** (C<sub>25</sub>H<sub>27</sub>N<sub>3</sub>) crystals were grown in mixture solution of DMSO and acetone. A suitable crystal was selected for experiments on the Bruker APEX-II CCD diffractometer. The crystal temperature was kept at 298.00 K during data acquisition. The structure was solved with the SHELXT structure solution program by Olex2 and Intrinsic Phasing. Using Least Squares minimization, the structure was optimized with the SHELXL refinement package.

### Preparation of stock solution and optical evaluation of analytes

A stock solution of probe **MDJ-O** (7.7 mg,  $4.0 \times 10^{-3}$  M) was prepared in 5.0 mL EtOH. Stock solutions of analytes, such as  $\text{Li}^+$ ,  $\text{Na}^+$ ,  $\text{Mg}^{2+}$ ,  $\text{K}^+$ ,  $\text{Ca}^{2+}$ ,  $\text{Cr}^{3+}$ ,  $\text{Fe}^{2+}$ ,  $\text{Co}^{2+}$ ,  $\text{Ni}^{2+}$ ,  $\text{Cu}^{2+}$ ,  $\text{Cd}^{2+}$ , I, Br, Cl,  $\text{S}^{2-}$ , PPI,  $\text{CN}^-$ ,  $\text{NO}_3^-$ ,  $\text{ClO}^-$ ,  $\text{HCO}_3^-$ ,  $\text{CH}_3\text{CO}_2^-$ , Cys, Hcy, GSH, Gly, Lys, Arg, ATP, Vitamin C, were dissolved in  $\text{H}_2\text{O}$  with the concentration of  $4.0 \times 10^{-2}$  M, separately.

All spectra were measured with a 1.0-cm-path-length cuvette and investigated between 400 and 900 nm wavelength range. The slit width of the exciting light and the emitting light was set as 5 nm.

### Dynamic light scattering (DLS) test

5  $\mu\text{L}$  of the **MDJ-O** stock solution was diluted with PBS buffer solution (10 mM, pH = 7.4, containing 2.5% EtOH, 1 mM CTAB) to 10  $\mu\text{M}$  as **MDJ-O** group.  $\text{Fe}^{2+}$  (100  $\mu\text{M}$ ) was added to **MDJ-O** (10  $\mu\text{M}$ ) solution as **MDJ-O** +  $\text{Fe}^{2+}$  group. The test was carried out by NanoBrook 90 Plus PALS (Brookhaven), the balance time was 10 min, the test temperature was 25  $^\circ\text{C}$ , and the measurements were carried out 5 times.

### Detection limit calculation

5  $\mu\text{L}$  of the **MDJ-O** stock solution was diluted with PBS buffer solution (10 mM, pH = 7.4, containing 2.5% EtOH, 1 mM CTAB) to a final concentration of 10  $\mu\text{M}$  as blank solution. The blank solution was prepared repeatedly for a total of 8 times. The fluorescence spectra and UV-vis absorption spectra were acquired after the solutions were well mixed. The fluorescence intensity of **MDJ-O** at 720 nm was selected and recorded as  $F_0$ , and the standard deviation ( $\delta$ ) was calculated according to the following formula. The limit of detection (LOD) of probe **MDJ-O** for  $\text{Fe}^{2+}$  was calculated using the equation of  $\text{LOD} = 3 \times \delta / S$ . The  $\delta$  in the equation is the standard deviation of the blank **MDJ-O** solution. The S is the slope of diverse concentrations of  $\text{Fe}^{2+}$  against the fluorescence intensity (720 nm) of **MDJ-O**. LOD was calculated by using the following linear equation:

$$\text{Linear Equation: } Y = 46.5462 X - 34.301 \quad R^2 = 0.9961 \quad S = 46.5462$$

$$\delta = \sqrt{\frac{\sum(F_0 - \bar{F}_0)^2}{n - 1}} = 47.8950 \quad n = 8, k = 3$$

$$\text{LOD} = K \times \delta / S = 3 \times 47.8950 / 46.5462 = 3.09 \times 10^{-6} \text{ M}$$

### HPLC study

One **MDJ** (10  $\mu\text{M}$ ) methanol solution and four **MDJ-O** (10  $\mu\text{M}$ ) methanol solutions were first prepared. Four **MDJ-O** (10  $\mu\text{M}$ ) methanol solutions were mixed with 0.5, 1, 2, and 5 equivalent  $\text{Fe}^{2+}$ , and then measured by HPLC. The column used for the HPLC measurement was the Accucore C18 column (150 nm  $\times$  4.6 mm). The mobile phase was mixed solution of methanol and water. During the elution process, the methanol content gradually increased from 40% to 95%. The elution time, flow rate, column temperature, injection sample size, and UV detection wavelength were 30 min, 0.8 mL/min, 35.8  $^{\circ}\text{C}$ , 5  $\mu\text{L}$ , and 380 nm, respectively.

### Density functional theory (DFT) calculations

DFT calculations was employed using the Gaussian 16 program. Geometry optimization was accomplished at B3LYP-D3BJ/TZVP level, in combination with the SMD implicit solvation model to take account of the solvation effect of DMSO. The orbitals and electrostatic potential mapped molecular surfaces were depicted using the VMD program.

### Cell culture

HepG2 cells were cultured in a carbon dioxide incubator (containing 5%  $\text{CO}_2$ ) at a temperature of 37  $^{\circ}\text{C}$ , allowing the cells to adhere and grow. The cells used in this work were all cultured 4-5 times after passage. All operations in the experiments were carried out on a super-clean workbench.

The experiments for exploring the ability of **MDJ-O** to visualize  $\text{Fe}^{2+}$  in living cells. HepG2 cells were cultured and used. The cells were divided into five groups: blank group, **MDJ-O** group, **MDJ-O** +  $\text{Fe}^{2+}$  group, Bpy + **MDJ-O** group, and Bpy +  $\text{Fe}^{2+}$  + **MDJ-O** group. First, HepG2 cells were incubated for 30 min with DMEM at 37  $^{\circ}\text{C}$  and imaged as control. Second, cells were treated with **MDJ-O** and they were incubated for 30 min at 37  $^{\circ}\text{C}$ , and then imaged as **MDJ-O** group. Third,  $\text{Fe}^{2+}$  was added to the cells and they were incubated for 30 min at 37  $^{\circ}\text{C}$ . After that, the cells were further treated with **MDJ-O** (10  $\mu\text{M}$ ) and then imaged as **MDJ-O** +  $\text{Fe}^{2+}$  group. Fourth, the cells were pretreated with 1 mM Bpy for 1 h. Then **MDJ-O** was added and incubated. After 30 min,

the cells were imaged as Bpy + **MDJ-O** group. Last, the cells were first pretreated with 1 mM Bpy for 1 h and then incubated with  $\text{Fe}^{2+}$  and **MDJ-O** for 30 min at 37 °C respectively. Finally, the cells were imaged as Bpy +  $\text{Fe}^{2+}$  + **MDJ-O** group. Cells were rinsed with PBS three times after each drug treatment. Laser scanning confocal microscope (TCS SP8 STED) imaging conditions: excitation wavelength was set as 561 nm, image acquisition channel was red channel (700-750 nm), and the scale was 25  $\mu\text{m}$ .

Cell colocalization experiment. Fluorescence imaging results were compared by co-staining the probe **MDJ-O** (10  $\mu\text{M}$ ) with commercially available Mito-Tracker (localization of mitochondria) and Lyso-Tracker (localization of lysosomes). Cells were divided into two groups: lysosome group and mitochondria group.

Lysosome group: the Lyso-Tracker (1 mM) stock solution was diluted 15,000 times with PBS buffer solution to be used as the Lyso-Tracker working solution. HepG2 cells were incubated in the medium containing **MDJ-O** (10  $\mu\text{M}$ ) for 30 min and then removed medium. After washing with PBS ( $\times 3$ ), Lyso-Tracker was added and incubated for 90 min. Then, the cells were imaged. Mitochondria group: the Mito-Tracker (1 mM) stock solution was diluted 5000 times with PBS buffer solution to be used as the Mito-Tracker working solution. HepG2 cells were incubated in the medium containing **MDJ-O** (10  $\mu\text{M}$ ) for 30 min at 37 °C, then the culture medium was removed and washed with PBS ( $\times 3$ ). After that, Mito-Tracker was added and incubated for 60 min at 37 °C. Finally, the fluorescence images were taken on the TCS SP8 STED confocal microscope. Image analysis was performed with ImageJ.

Flow cytometry analysis. HepG2 cells were inoculated at a density of  $5 \times 10^5$  cells/well on 6-well plates and cultured overnight. The prepared cells were divided into five groups: blank group, **MDJ-O** group, **MDJ-O** +  $\text{Fe}^{2+}$  group, Bpy + **MDJ-O** group, and Bpy +  $\text{Fe}^{2+}$  + **MDJ-O** group. HepG2 cells were incubated in DMEM at 37 °C for 30 min as blank group. **MDJ-O** (10  $\mu\text{M}$ ) was added to the cells and incubated for 30 minutes as **MDJ-O** group. The cells were added with 100  $\mu\text{M}$   $\text{Fe}^{2+}$  and incubated for 30 min, then the cells were added with **MDJ-O** (10  $\mu\text{M}$ ) and incubated for 30 min as **MDJ-O** +  $\text{Fe}^{2+}$  group. The cells were pretreated with 1 mM Bpy for 1 h, then **MDJ-O** (10  $\mu\text{M}$ ) was added and incubated for 30 min as Bpy + **MDJ-O** group. The cells were first pretreated with 1 mM Bpy for 1 h, then incubated with  $\text{Fe}^{2+}$  and **MDJ-O** for 30 min in turn, and were classified as Bpy +  $\text{Fe}^{2+}$  + **MDJ-O** group. Cells were washed with PBS ( $\times 3$ ) after each drug

treatment. Five groups of cells were digested and centrifuged, and then PBS (2 mL) was added for resuspension. After centrifugation again, PBS (1 mL) was added for resuspension. After filtering, the samples were tested by BD FACSymphony multiparameter flow cytometer (BD, USA). Sample detection speed:  $\geq 40000$  cells/s. The excitation wavelength was selected at 561 nm. Fluorescence detection sensitivity: FITC $<80$  MESF, PE $<30$  MESF, PE-Cy5 $<10$  MESF, APC $<70$  MESF. Fluorescence signal resolution: 262144 (18bit).

### ***In vivo* imaging of zebrafish**

The adult zebrafish imaging experiments. The zebrafish were divided into three groups: blank group, **MDJ-O** group, and **MDJ-O + Fe<sup>2+</sup>** group. For the first group, the zebrafish were incubated for 30 min at room temperature in the water, and then they were washed with water for 5 minutes and then killed by ice bath as blank group. For the second group, the adult zebrafish were incubated in PBS buffer containing 10  $\mu$ M **MDJ-O** for 30 minutes at room temperature. Then the zebrafish were washed with water for 5 minutes and then killed by ice bath as **MDJ-O** group. In the third group, the adult zebrafish were incubated with **MDJ-O** (10  $\mu$ M) solution for 30 min and washed with Wahaha water. 5 min later, and the zebrafish were incubated with 100  $\mu$ M Fe<sup>2+</sup> for 30 min at room temperature. After being washed in water, the zebrafish were killed by ice bath as **MDJ-O + Fe<sup>2+</sup>** group to be tested. Imaging conditions for zebrafish were as follows: excitation and emission wavelengths were at 535 nm and 720 nm respectively.

### ***In vivo* imaging of mice**

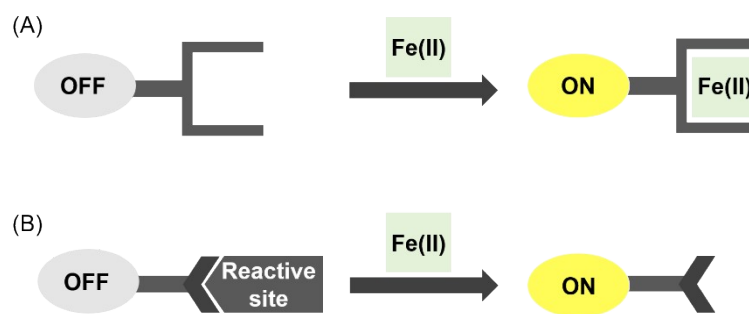
Kunming mouse (20  $\pm$  2 g) was selected as another experimental animal model. After anesthesia, the mice were separated into two groups. The control group was intramuscularly injected **MDJ-O** (100  $\mu$ M, 50  $\mu$ L) into the right leg, and the imaging was performed 5 minutes later. In the experimental group, **MDJ-O** (100  $\mu$ M, 50  $\mu$ L) was injected into the right leg of mice, and FeSO<sub>4</sub> (1 mM, 50  $\mu$ L) solution was injected into the same position for imaging after 5 minutes. Each group was imaged using three mice with an excitation wavelength of 535 nm, and the images were captured at an emission wavelength of 720 nm.

### **Imaging of Fe<sup>2+</sup> in APAP-induced liver and kidney injury**



Kunming mice were divided into three groups. Mice in the first group were injected with **MDJ-O** (100  $\mu$ M, 100  $\mu$ L) through tail vein. After 30 min, the heart, lung, spleen, liver, and kidney of the mice were removed for imaging. Mice in the second group were injected with APAP (300 mg/kg, 300  $\mu$ L) through the tail vein. After 3 h, probe **MDJ-O** (100  $\mu$ M, 100  $\mu$ L) was injected. 30 min later, the liver and kidney were taken out from the mice for imaging. In the third group, APAP (300 mg/kg, 300  $\mu$ L) was first injected through the tail vein. 3 hours later, Bpy (10 mM, 100  $\mu$ L) was injected, and then **MDJ-O** (100  $\mu$ M, 100  $\mu$ L) was injected 1 hour later. Finally, the liver and kidney of the mice were taken out for imaging 30 min later. The imaging excitation wavelength was at 535 nm, and the images were captured at the emission wavelength of 720 nm.

The heart, lung, spleen, liver, and kidney of mice in the blank group and **MDJ-O** + Fe<sup>2+</sup> group were dissected for tissue section analysis. After being fixed with 4% paraformaldehyde, they were prepared according to the procedures of pruning, dehydration, embedding, slicing, dyeing, and sealing. Finally, the tissue sections were viewed under the microscope at different multiples.



**Scheme S1.** Main fluorescent probe types for Fe<sup>2+</sup>.

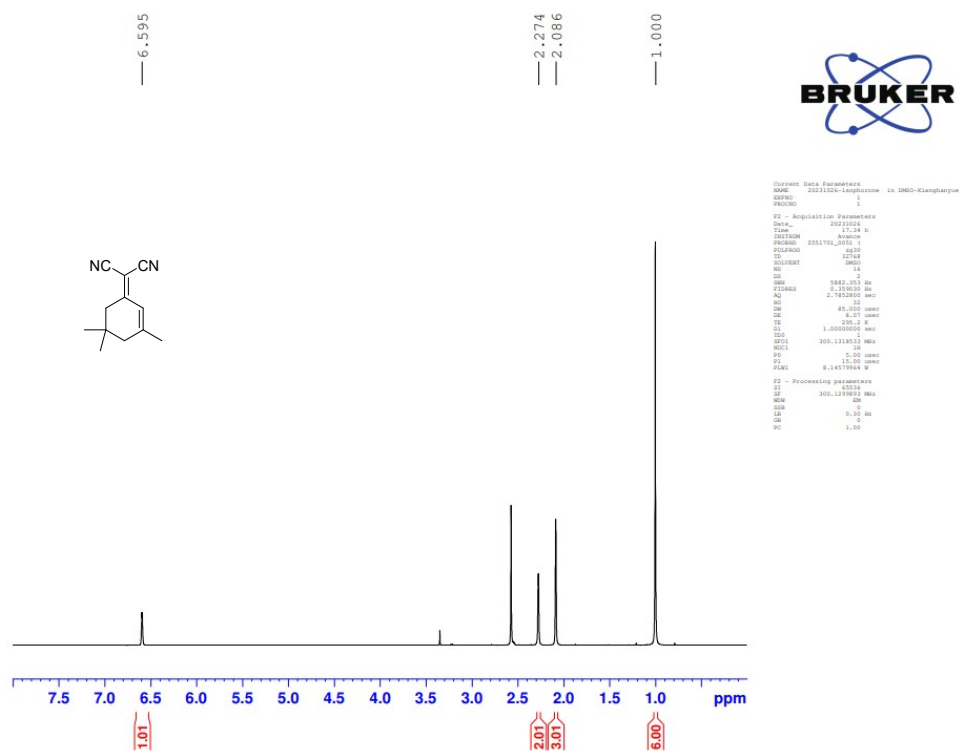


**Fig. S1.** <sup>1</sup>H NMR spectrum of **1** in DMSO-*d*<sub>6</sub>.

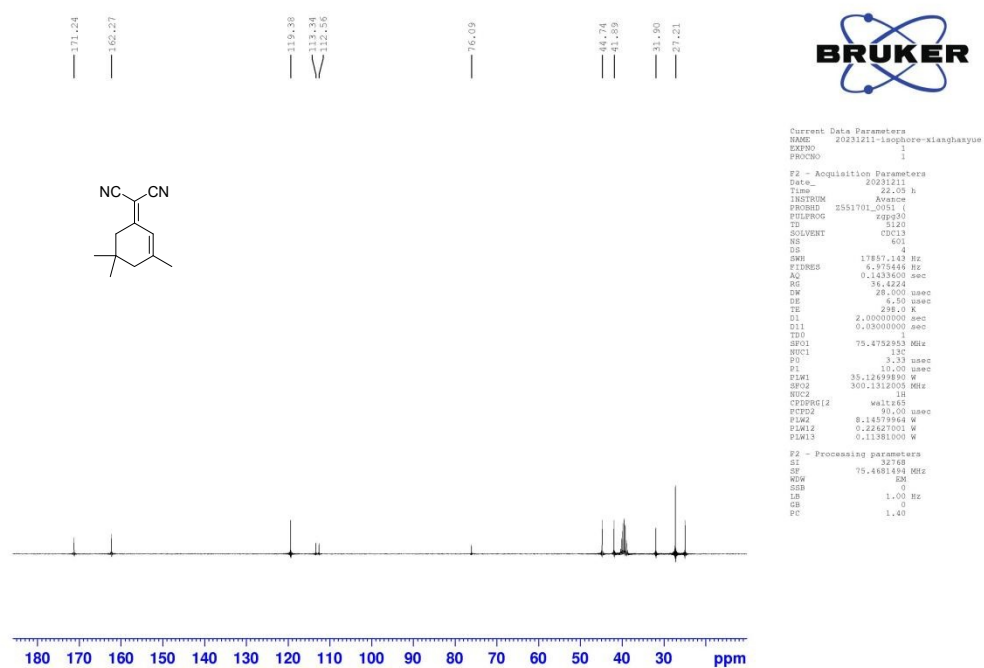


Fig. S2.  $^{13}\text{C}$  NMR spectrum of **1** in  $\text{DMSO-}d_6$ .

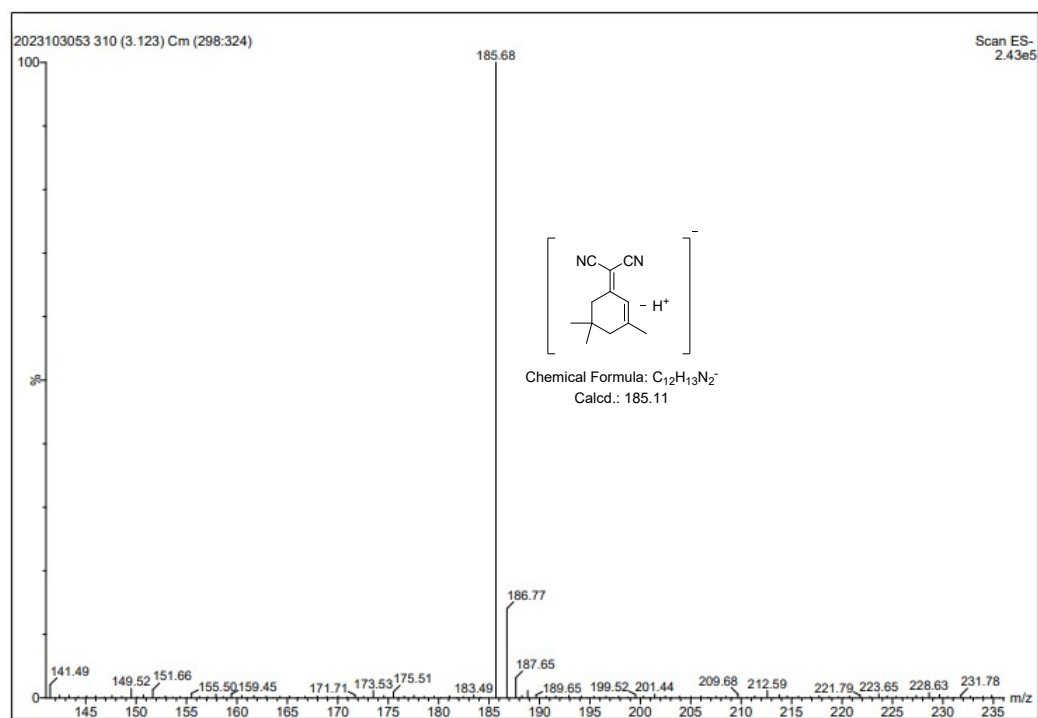


Fig. S3. ESI-MS spectrum of **1** in negative mode. ESI-MS( $m/z$ ): 185.68 [**1** -  $\text{H}^+$ ] (cacl. for  $\text{C}_{12}\text{H}_{13}\text{N}_2^-$ : 185.11).

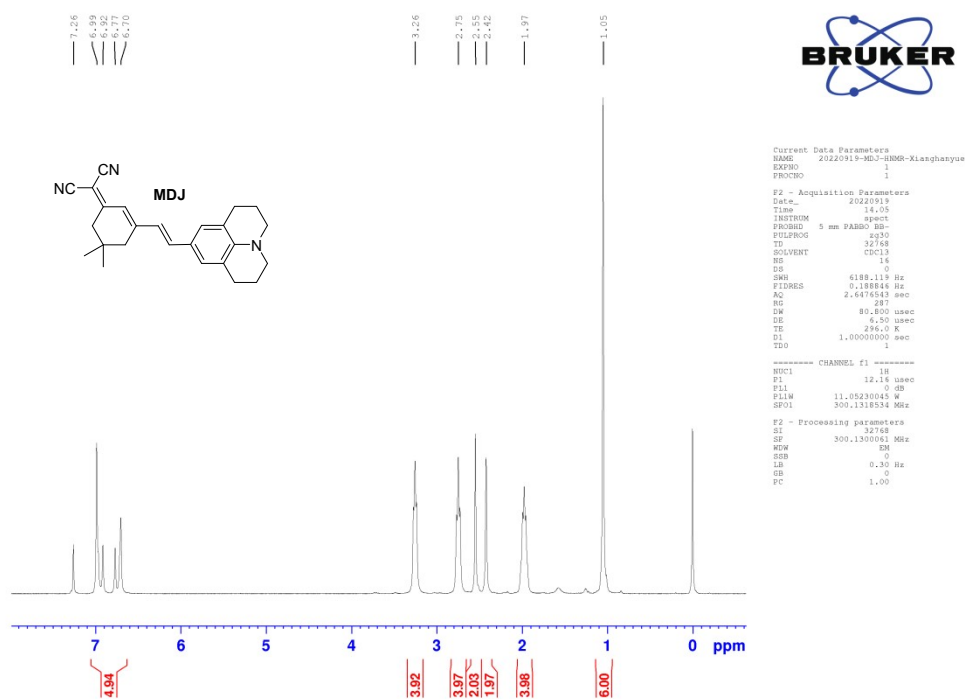


Fig. S4. <sup>1</sup>H NMR spectrum of MDJ in CDCl<sub>3</sub>.

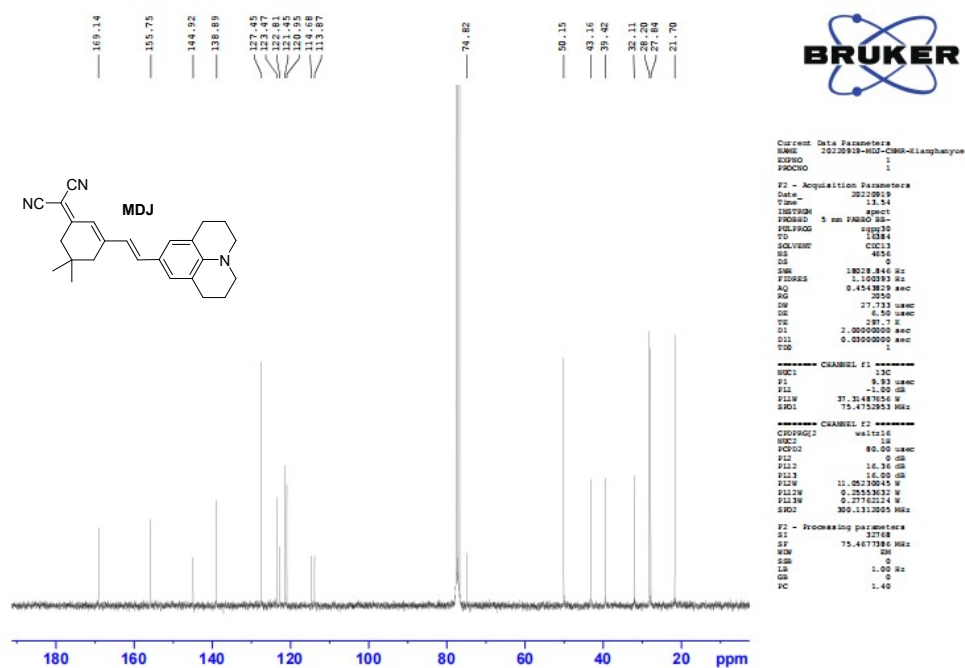
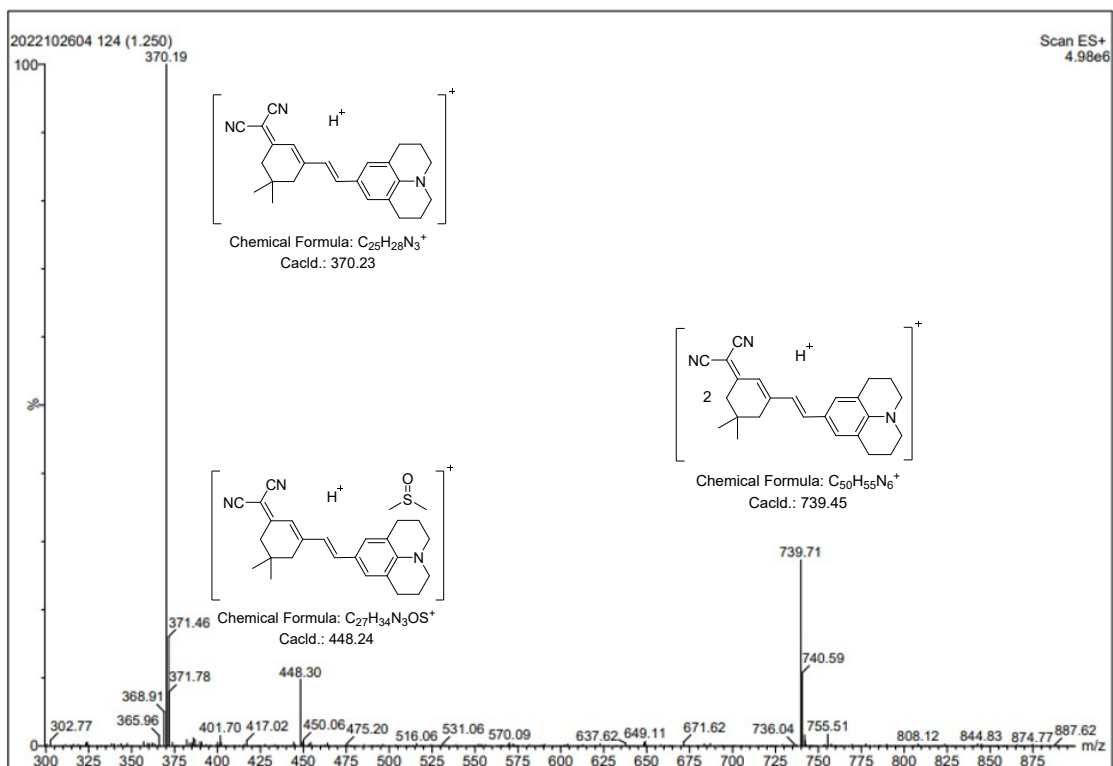
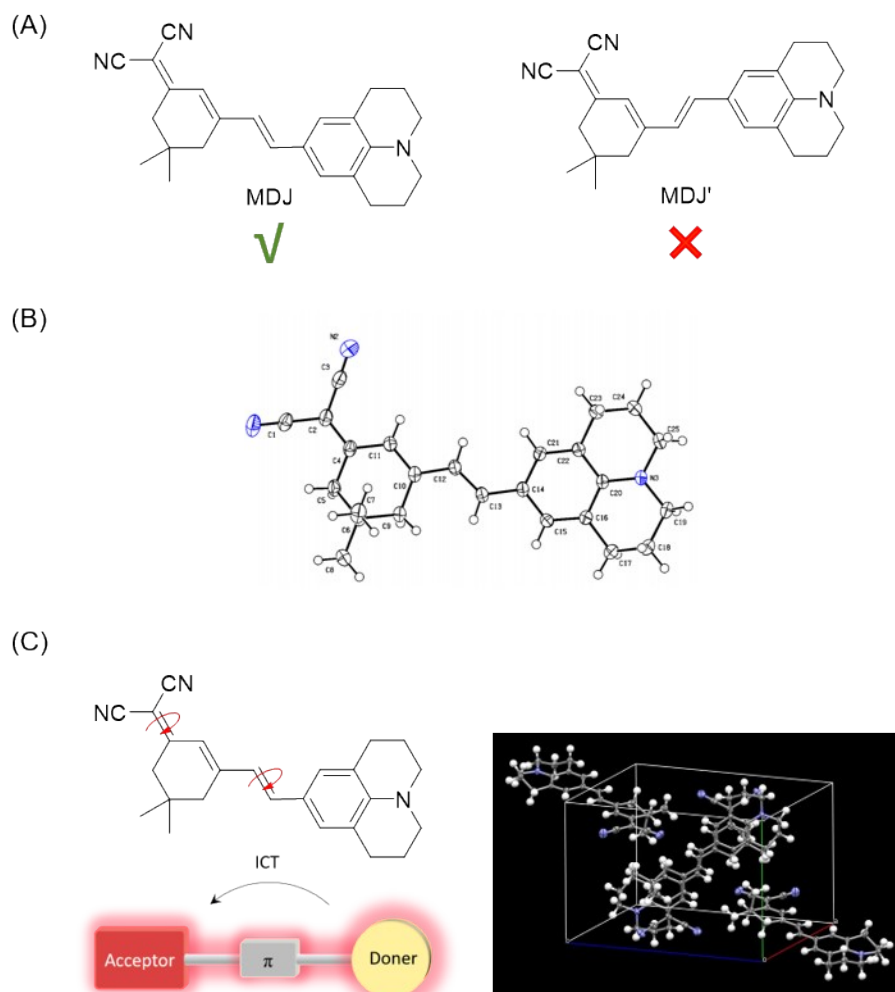


Fig. S5. <sup>13</sup>C NMR spectrum of MDJ in CDCl<sub>3</sub>.



**Fig. S6.** ESI-MS spectrum of **MDJ** in positive mode. ESI-MS ( $m/z$ ): 370.19 [**MDJ** +  $H^+$ ] $^+$  (cacl. for  $C_{25}H_{28}N_3^+$ : 370.23), ESI-MS( $m/z$ ): 448.30 [**MDJ** + DMSO +  $H^+$ ] $^+$  (cacl. for  $C_{27}H_{34}N_3OS^+$ : 448.24), ESI-MS( $m/z$ ): 739.71 [2 **MDJ** +  $H^+$ ] $^+$  (cacl. for  $C_{50}H_{55}N_6^+$ : 739.45).



**Fig. S7.** X-ray crystal structure of **MDJ**. (A) Chemical structure of **MDJ** and its potential isomer **MDJ'**. (B) X-ray crystal structure of **MDJ**. (C) D- $\pi$ -A type crystal structure and unit cell of **MDJ**.

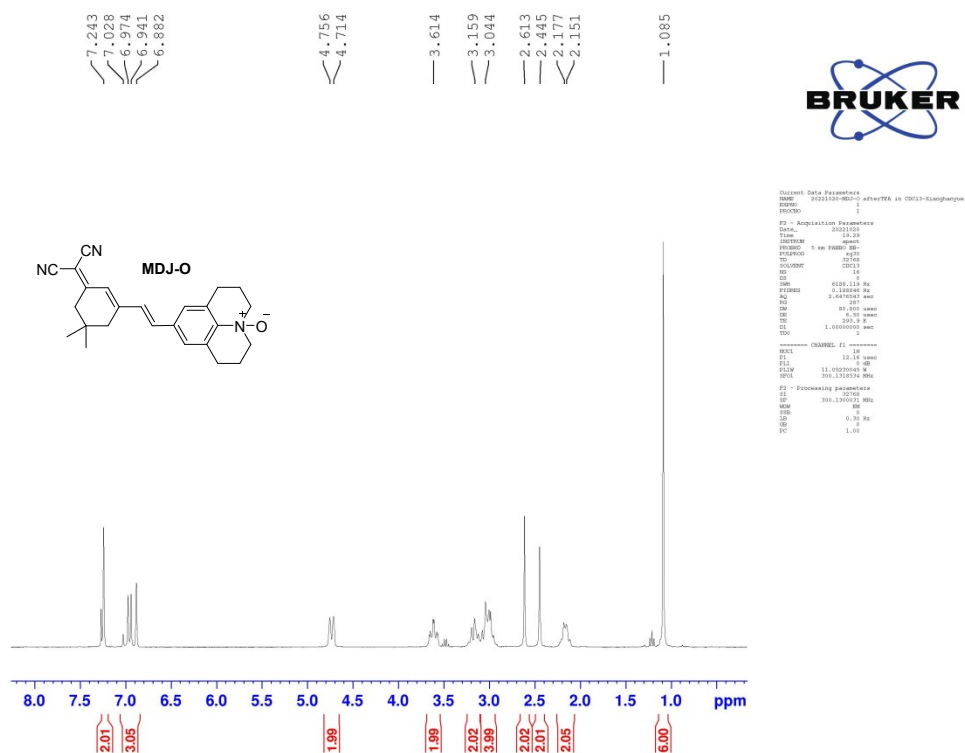


Fig. S8. <sup>1</sup>H NMR spectrum of MDJ-O in CDCl<sub>3</sub>.

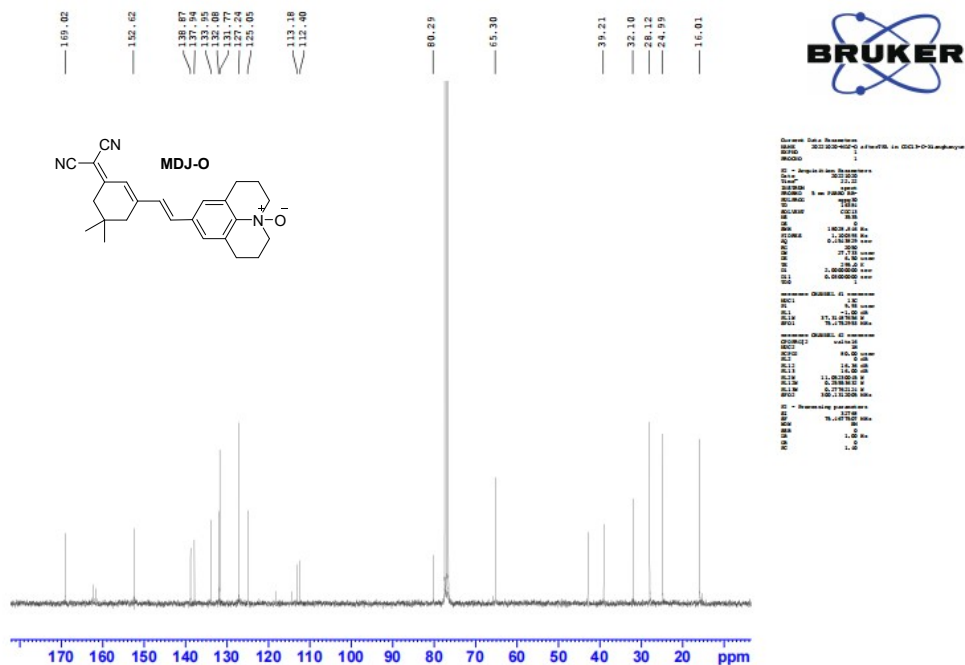
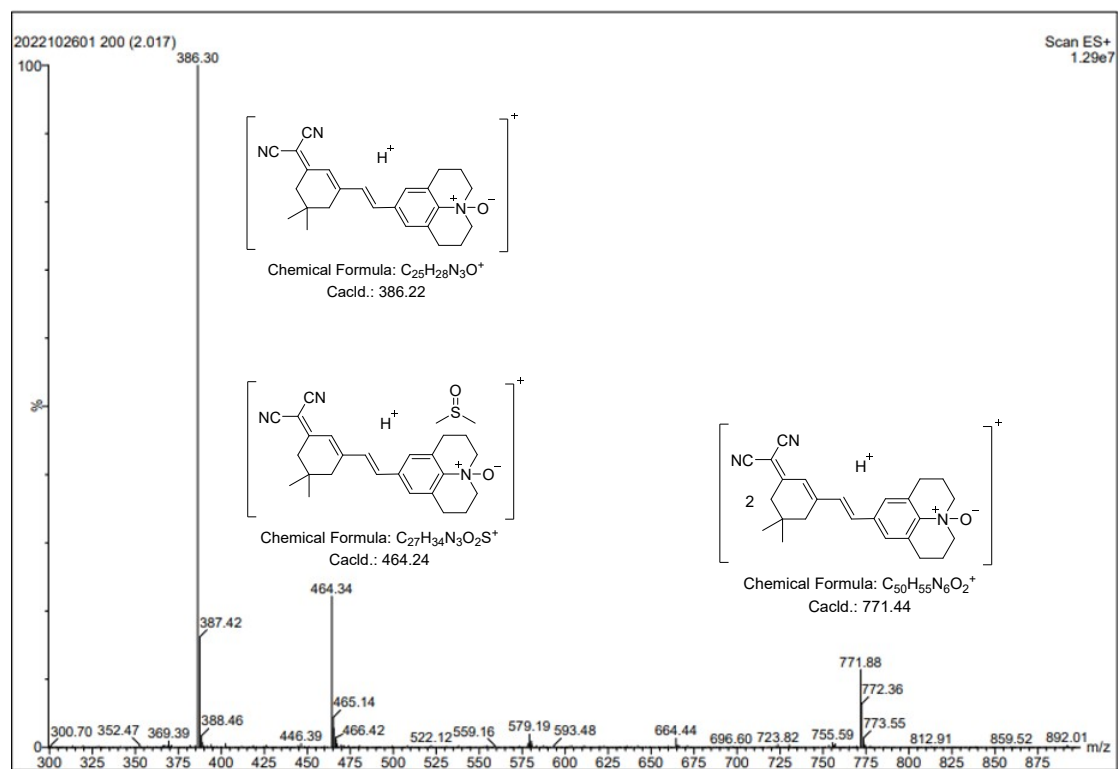
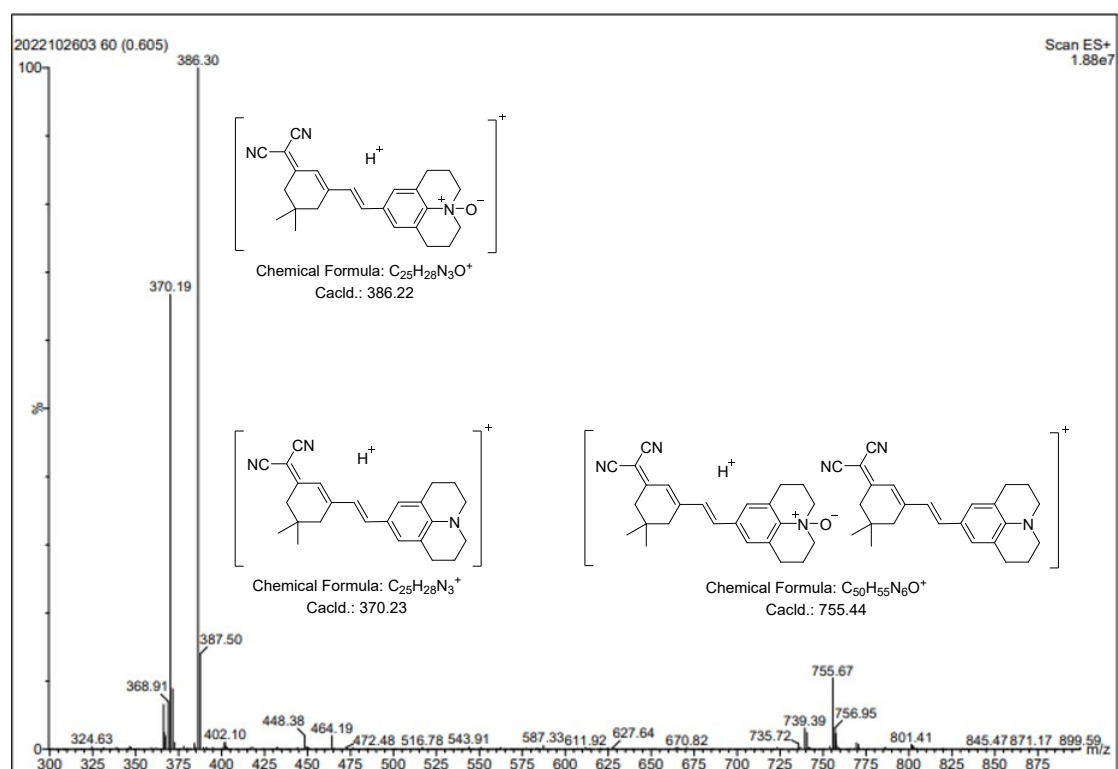


Fig. S9. <sup>13</sup>C NMR spectrum of MDJ-O in CDCl<sub>3</sub>.



**Fig. S10.** ESI-MS spectrum of **MDJ-O** in positive mode. ESI-MS ( $m/z$ ) 386.30 [**MDJ-O** +  $H^+$ ]<sup>+</sup> (cacl. for  $C_{25}H_{28}N_3O^+$ : 386.22), ESI-MS( $m/z$ ): 464.34 [**MDJ-O** + DMSO +  $H^+$ ]<sup>+</sup> (cacl. for  $C_{27}H_{34}N_3OS^+$ : 464.24), ESI-MS( $m/z$ ): 771.88 [2 **MDJ-O** +  $H^+$ ]<sup>+</sup> (cacl. for  $C_{50}H_{55}N_6^+$ : 771.44).





**Fig. S11.** ESI-MS spectrum of **MDJ-O** in the presence of  $\text{Fe}^{2+}$ . ESI-MS ( $m/z$ ): 370.19 [**MDJ** +  $\text{H}^+$ ]<sup>+</sup> (cacl. for  $\text{C}_{25}\text{H}_{28}\text{N}_3^+$ : 370.23), ESI-MS ( $m/z$ ) 386.30 [**MDJ-O** +  $\text{H}^+$ ]<sup>+</sup> (cacl. for  $\text{C}_{25}\text{H}_{28}\text{N}_3\text{O}^+$ : 386.22), ESI-MS( $m/z$ ): 755.67 [**MDJ-O** + **MDJ** +  $\text{H}^+$ ]<sup>+</sup> (cacl. for  $\text{C}_{50}\text{H}_{55}\text{N}_6^+$ : 755.44).

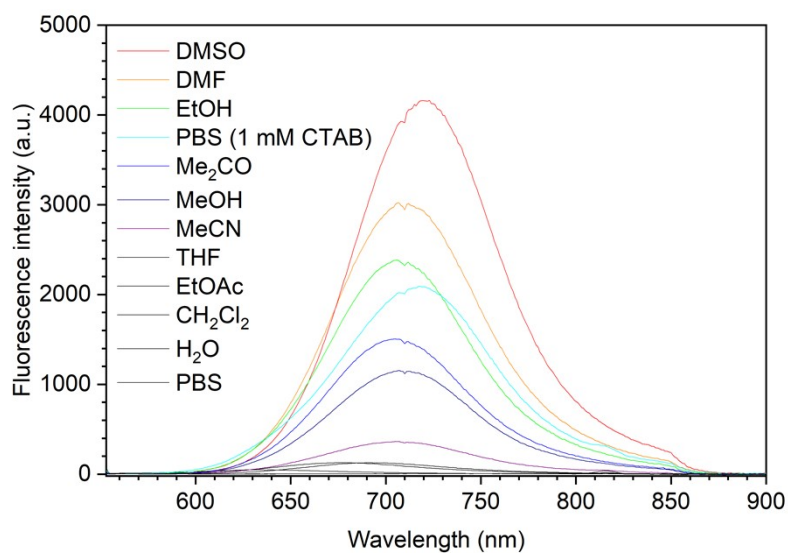


**Fig. S12.** Fluorescence spectra of 10  $\mu\text{M}$  probe **MDJ-O** upon adding 100  $\mu\text{M}$   $\text{Fe}^{2+}$  in various solvents.

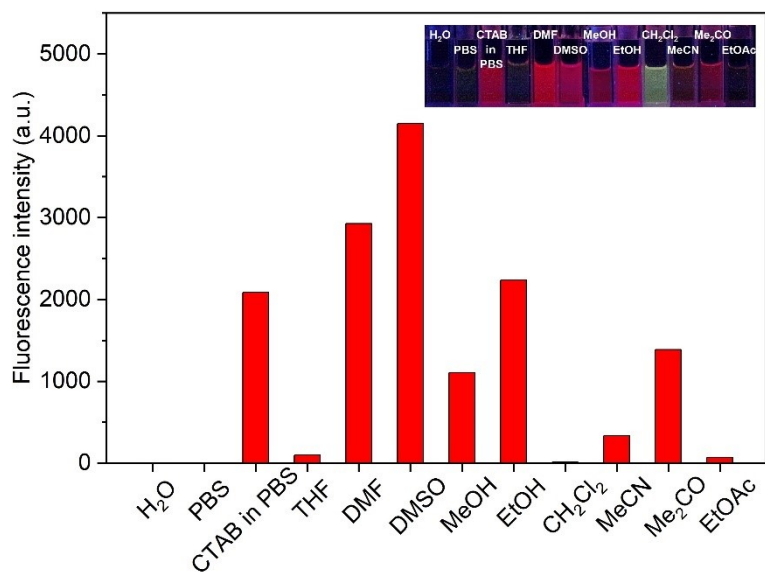


**Fig. S13.** The bar graph comparison of the fluorescence intensities of  $10 \mu\text{M}$  probe **MDJ-O** after adding  $100 \mu\text{M}$   $\text{Fe}^{2+}$  in various solvents such as  $\text{H}_2\text{O}$ , PBS, CTAB in PBS, THF, DMF, DMSO, MeOH, EtOH,  $\text{CH}_2\text{Cl}_2$ , MeCN,  $\text{Me}_2\text{CO}$ , EtOAc. Inset: the fluorescence image of **MDJ-O** with the addition of  $\text{Fe}^{2+}$  in various solvents under 365 nm UV light.

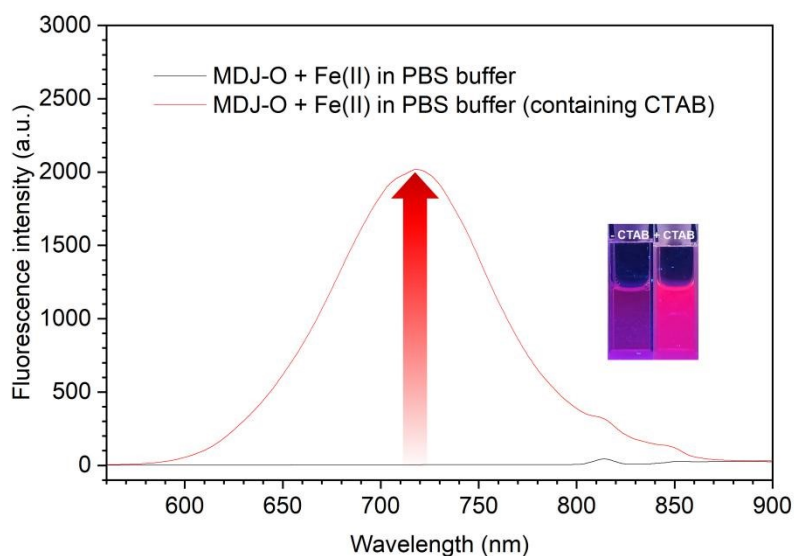


**Fig. S14.** Fluorescence spectra of  $10 \mu\text{M}$  probe **MDJ-O** upon adding  $100 \mu\text{M}$   $\text{Fe}^{2+}$  in various solvents. Red line: fluorescence spectrum of  $10 \mu\text{M}$  probe **MDJ-O** after adding  $100 \mu\text{M}$   $\text{Fe}^{2+}$  in PBS buffer (10 mM, pH = 7.4, containing 2.5% EtOH, 1 mM CTAB). Black line: fluorescence spectrum of  $10 \mu\text{M}$  probe **MDJ-O** after adding  $100 \mu\text{M}$   $\text{Fe}^{2+}$  in PBS buffer (10 mM, pH = 7.4, containing 2.5% EtOH).

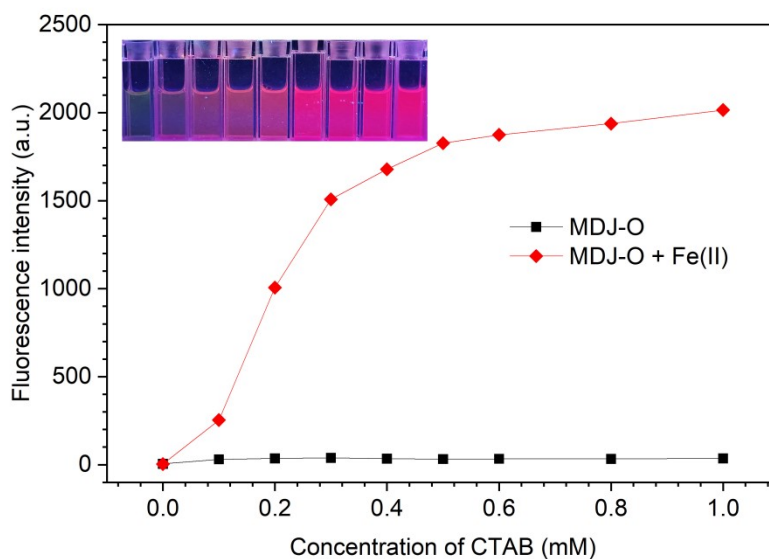


**Fig. S15.** Fluorescence emission intensities of probe **MDJ-O** (10  $\mu\text{M}$ ) response to  $\text{Fe}^{2+}$  (100  $\mu\text{M}$ ) in PBS buffer containing increasing concentrations CTAB (0 – 1 mM). Inset: the fluorescence image of **MDJ-O** with the addition of  $\text{Fe}^{2+}$  in PBS buffer containing various concentrations CTAB (0 – 1 mM) under 365 nm UV light.

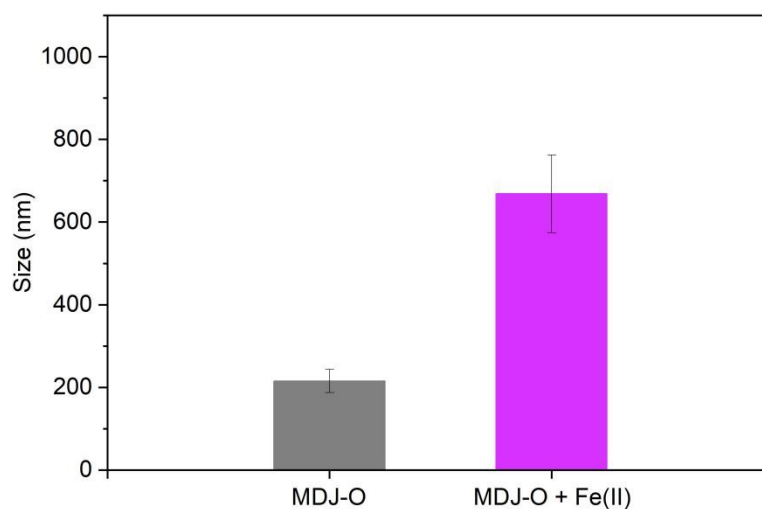


**Fig. S16.** The size distribution of **MDJ-O** (10  $\mu\text{M}$ ) dispersed in PBS buffer (10 mM, pH = 7.4, containing 2.5% EtOH, 1 mM CTAB) with or without adding  $\text{Fe}^{2+}$  (100  $\mu\text{M}$ ).

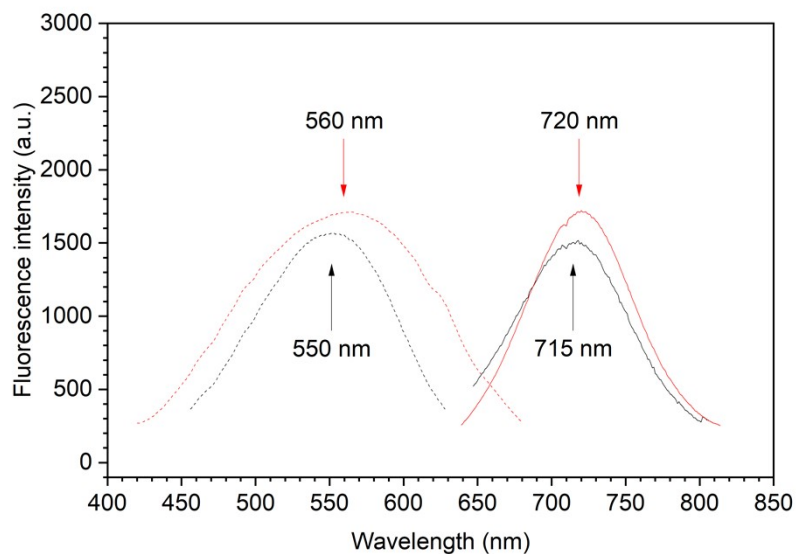


**Fig. S17.** Fluorescence excitation spectra and emission spectra of 10  $\mu\text{M}$  **MDJ** (black line) and 10  $\mu\text{M}$  **MDJ-O** after the reaction with  $\text{Fe}^{2+}$  (red line) in PBS buffer (10 mM, pH = 7.4, containing 2.5% EtOH, 1 mM CTAB).

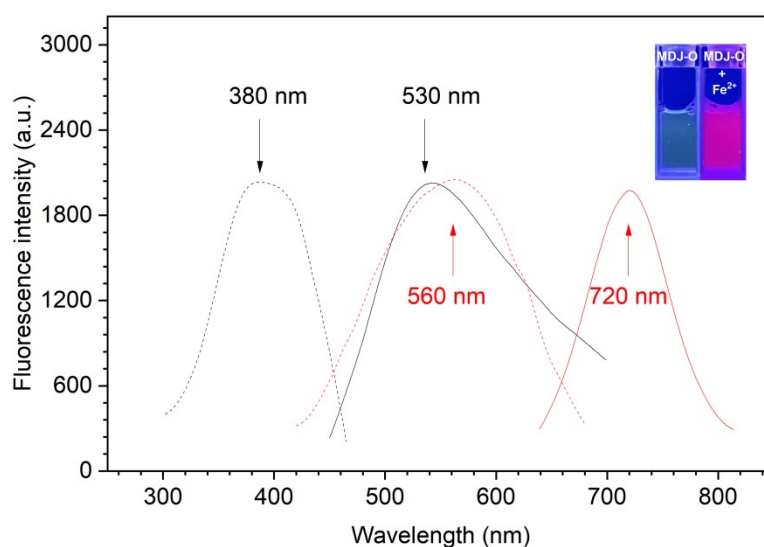


**Fig. S18.** Fluorescence excitation spectra and emission spectra of 10  $\mu\text{M}$  **MDJ-O** (black line) and 10  $\mu\text{M}$  **MDJ-O** after the reaction with  $\text{Fe}^{2+}$  (red line) in PBS buffer (10 mM, pH = 7.4, containing 2.5% EtOH, 1 mM CTAB).

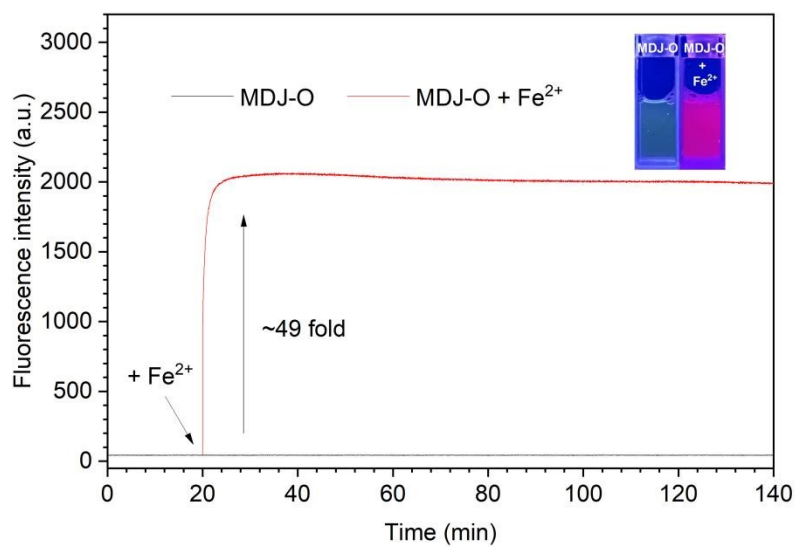


**Fig. S19.** Time-trace plot of fluorescence intensities of **MDJ-O** (10  $\mu\text{M}$ ) upon treated with  $\text{Fe}^{2+}$  (100  $\mu\text{M}$ ) in PBS buffer (10 mM, pH = 7.4, containing 2.5% EtOH, 1 mM CTAB). The fluorescence intensity was monitored at  $\lambda_{\text{ex}} = 540 \text{ nm}$  and  $\lambda_{\text{em}} = 720 \text{ nm}$ , respectively.

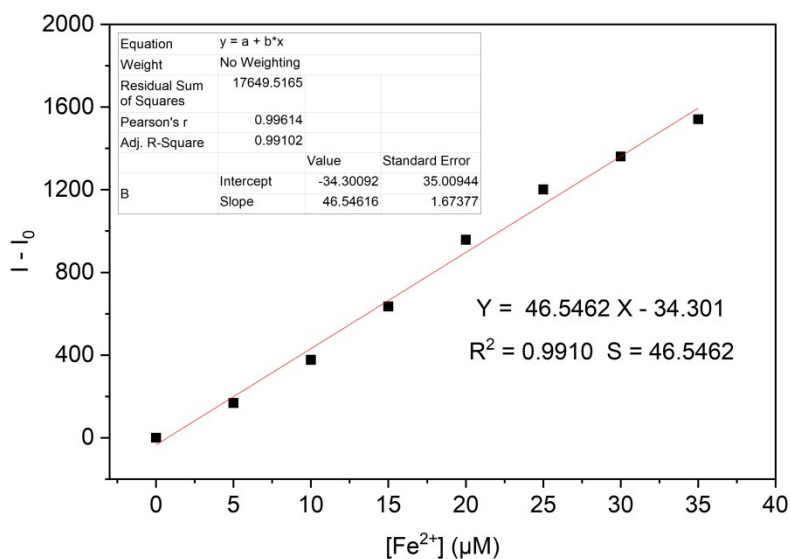


**Fig. S20.** The limit of detection (LOD) of **MDJ-O** towards  $\text{Fe}^{2+}$  was determined from the following equation:  $C_{\text{LOD}} = k \times \delta / S$ , where  $k = 3$ ;  $\delta$  is the standard deviation of the blank solution (2.5601);  $S$  is the slope of the calibration curve.

The result of the analysis is as follows:

Linear Equation:  $Y = 46.5462 X - 34.301$        $R^2 = 0.9961$        $S = 46.5462$

$$\delta = \sqrt{\frac{\sum (F_0 - \bar{F}_0)^2}{n - 1}} = 47.8950 \quad n = 8, k = 3$$

$$\text{LOD} = K \times \delta / S = 3 \times 47.8950 / 46.5462 = 3.09 \times 10^{-6} \text{ M}$$

$F_0$  is the fluorescence intensity at 720 nm of **MDJ-O**.

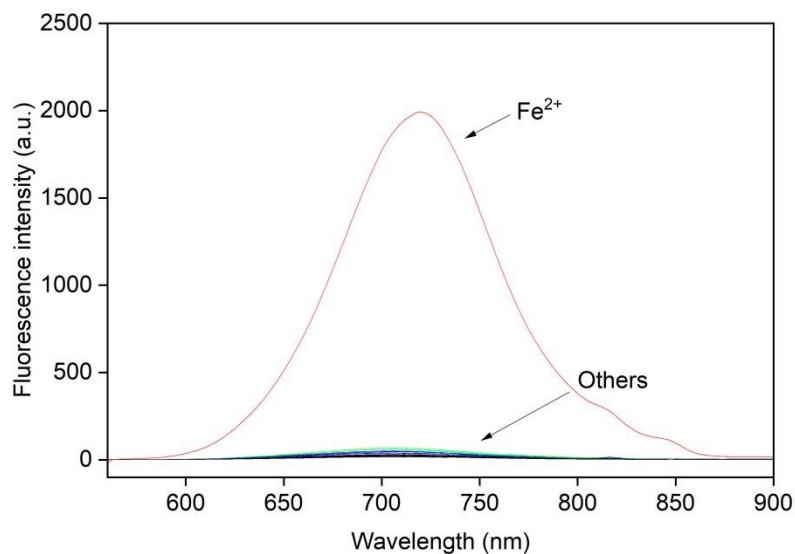


**Fig. S21.** Fluorescent spectra of **MDJ-O** (10  $\mu\text{M}$ ) upon the addition of 10 equiv. of various analytes in PBS buffer (10 mM, pH = 7.4, containing 2.5% EtOH, 1 mM CTAB). The fluorescence intensity was monitored at  $\lambda_{\text{ex}} = 540 \text{ nm}$ .

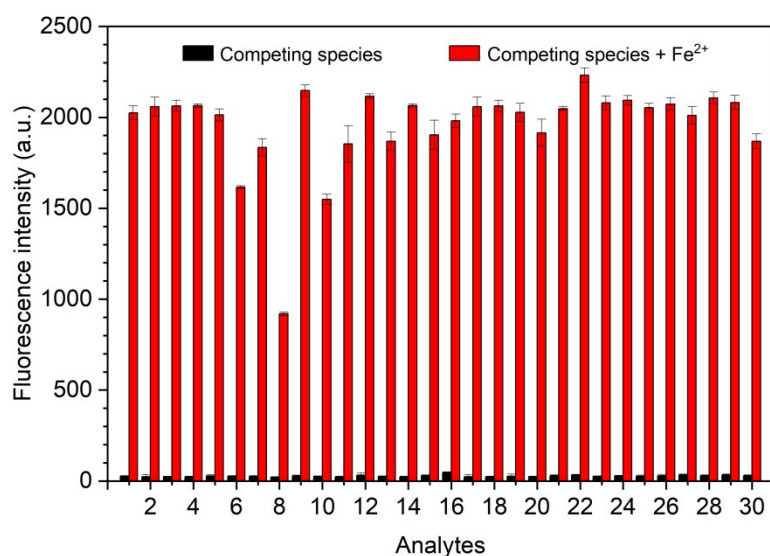


**Fig. S22.** The bar graph comparison of the fluorescence intensities of **MDJ-O** (10  $\mu\text{M}$ ) towards  $\text{Fe}^{2+}$  (100  $\mu\text{M}$ ) after the addition of 10 equiv. of various analytes (1, Blank; 2,  $\text{Na}^+$ ; 3,  $\text{K}^+$ ; 4,  $\text{Ca}^{2+}$ ; 5,  $\text{Mg}^{2+}$ ; 6,  $\text{Cr}^{2+}$ ; 7,  $\text{Co}^{2+}$ ; 8,  $\text{Cu}^{2+}$ ; 9,  $\text{Cd}^{2+}$ ; 10,  $\text{Mn}^{2+}$ ; 11,  $\text{Ni}^{2+}$ ; 12,  $\text{Fe}^{3+}$ ; 13,  $\text{I}^-$ ; 14,  $\text{Cl}^-$ ; 15,  $\text{Br}^-$ ; 16,  $\text{HS}^-$ ; 17,  $\text{NO}_3^-$ ; 18,  $\text{SO}_4^{2-}$ ; 19,  $\text{ClO}^-$ ; 20,  $\text{HCO}_3^-$ ; 21,  $\text{H}_2\text{PO}_4^{2-}$ ; 22, ATP; 23, Arg; 24, Lys; 25, Glu; 26, Gly; 27, Cys; 28, Hcy; 29, GSH; 30, Vitamin C) in PBS buffer (10 mM, pH = 7.4, containing 2.5% EtOH, 1 mM CTAB). Error bars represent the standard deviation from triplicate experiments.  $\lambda_{\text{ex}} = 540 \text{ nm}$ .

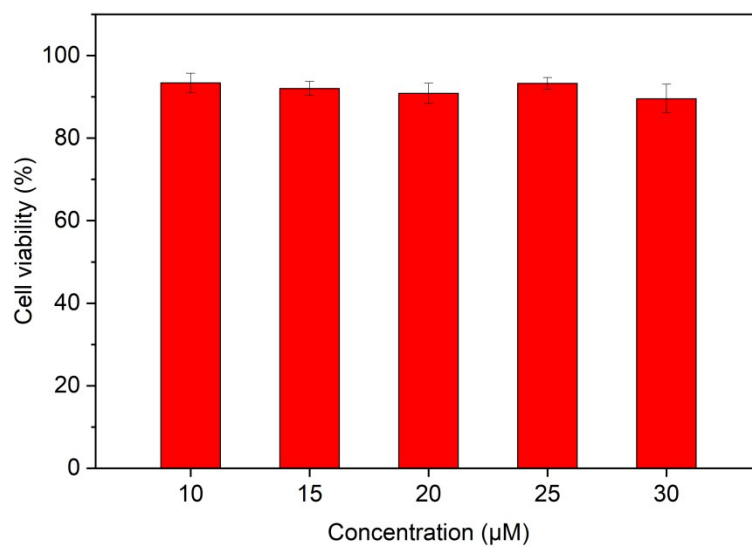


**Fig. S23.** A MTT assay shows the percentage of viable HepG2 cells after treatment with different concentrations of probe **MDJ-O** (10, 15, 20, 25, 30 µM) for 24 hours.

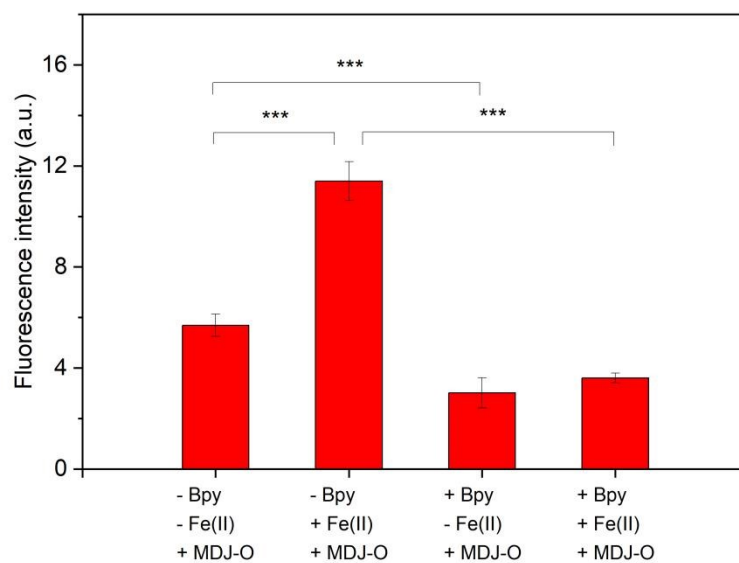


**Fig. S24.** Mean fluorescence intensities observed by confocal imaging Figure 4B. Statistical analyses were performed with a Student's t-test. \*\*P < 0.01, \*\*\*P < 0.001 (n = 3). Error bars indicate ± S.E.M.



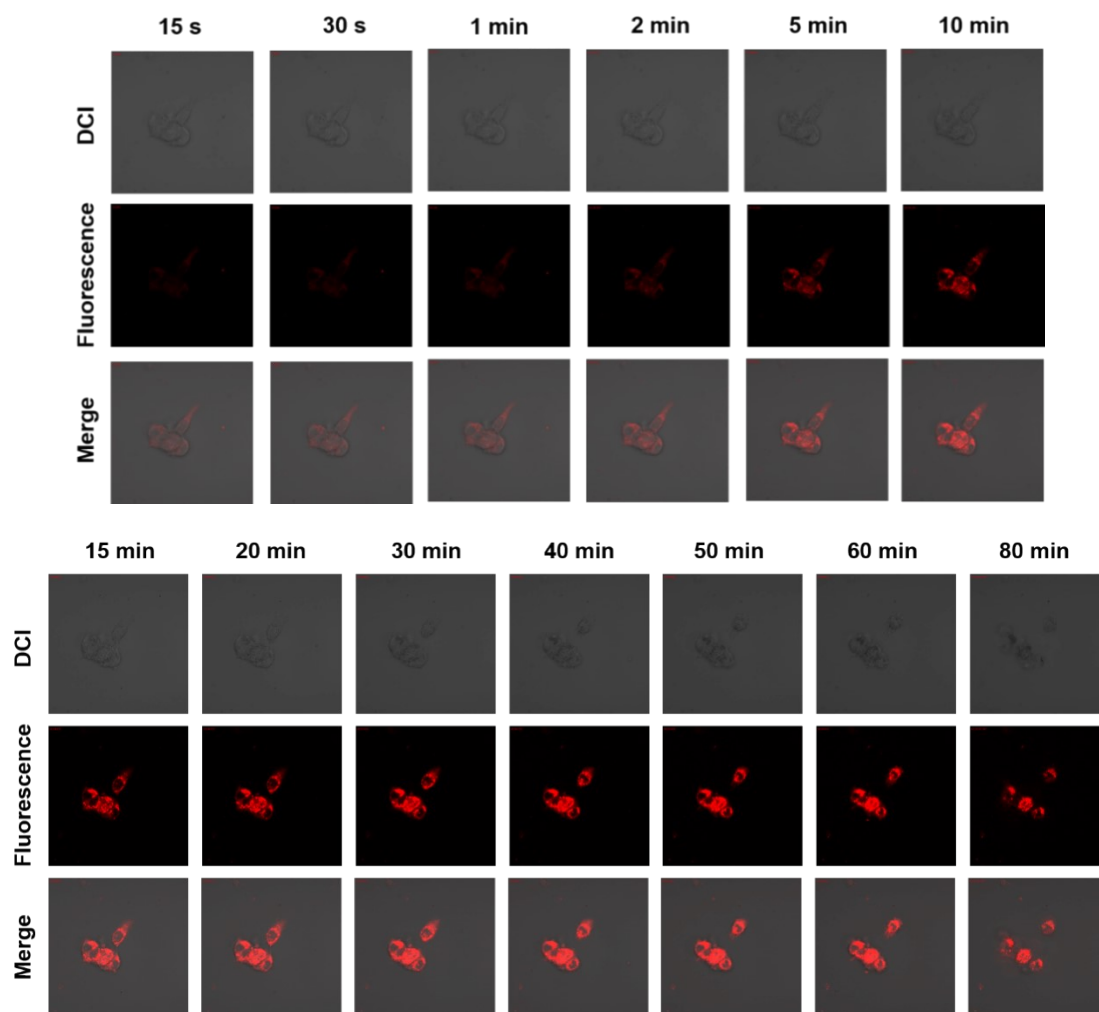


**Fig. S25.** The photostability of **MDJ-O** in living cells. Cells were pretreated with  $\text{Fe}^{2+}$  and then incubated with **MDJ-O** (10  $\mu\text{M}$ ). HepG2 cells were continuously illuminated at 561 nm for 80 min.  $\lambda_{\text{em}} = 660\text{--}720$  nm. Scale bar = 25  $\mu\text{m}$ .

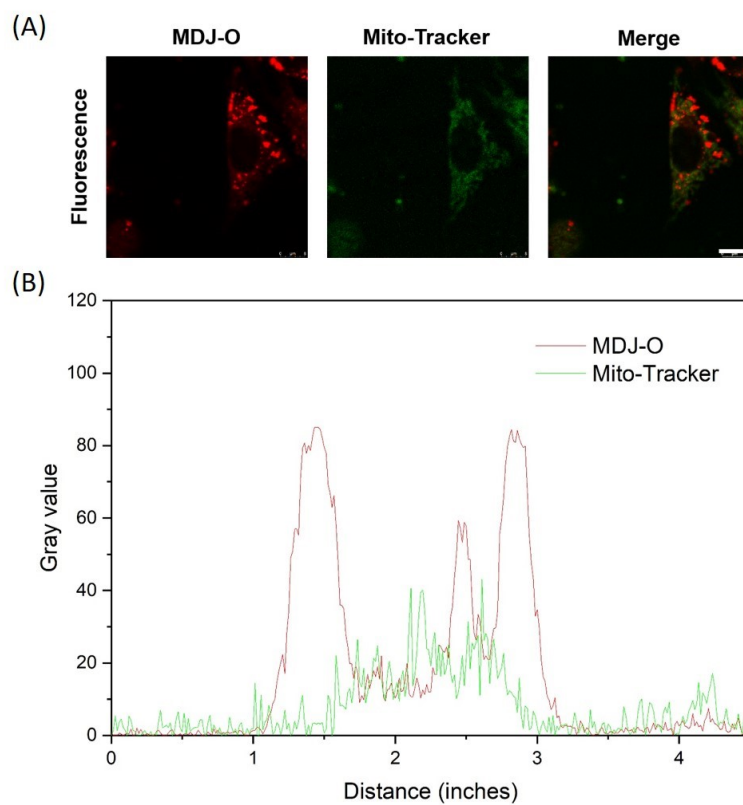


**Fig. S26.** (A) Co-localization imaging of HepG2 cells. From left to right: the cells were stained with **MDJ-O**, the cells were stained with Mito-Tracker, merged image. Green channel:  $\lambda_{\text{ex}} = 488$  nm,  $\lambda_{\text{em}} = 500\text{--}550$  nm. Red channel:  $\lambda_{\text{ex}} = 561$  nm,  $\lambda_{\text{em}} = 660\text{--}720$  nm. (B) The intensity profile of the cells.

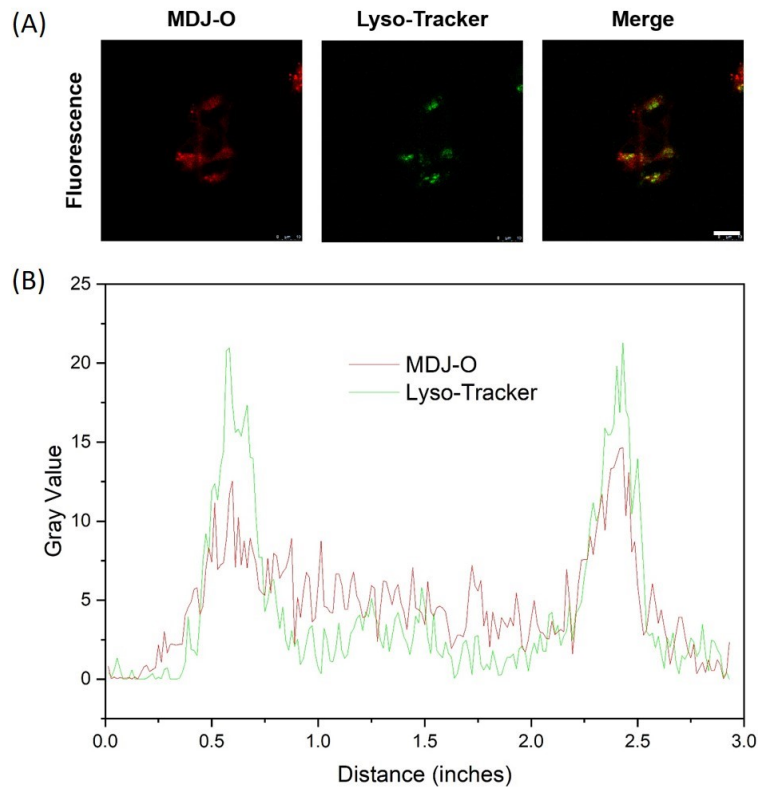


**Fig. S27.** Co-localization imaging of HepG2 cells. From left to right: the cells were stained with **MDJ-O**, the cells were stained with Lyso-Tracker, merged image. Green channel:  $\lambda_{\text{ex}} = 488$  nm,  $\lambda_{\text{em}} = 500\text{--}550$  nm. Red channel:  $\lambda_{\text{ex}} = 561$  nm,  $\lambda_{\text{em}} = 660\text{--}720$  nm. (B) The intensity profile of the cells.

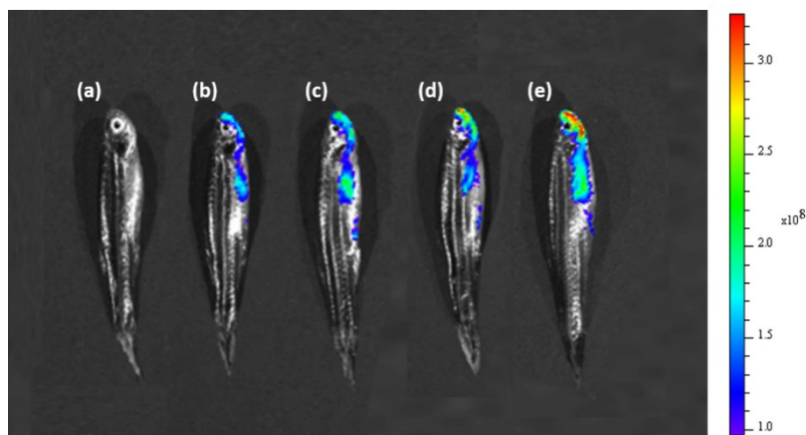


**Fig. S28.** Fluorescence images of zebrafish: (a) Blank control group. (b) **MDJ-O** (10  $\mu\text{M}$ ) control group. (c) - (e) Zebrafish samples pretreated with  $\text{Fe}^{2+}$  (10  $\mu\text{M}$ , 20  $\mu\text{M}$ , 50  $\mu\text{M}$ ) for 30 min before incubation with **MDJ-O** (10  $\mu\text{M}$ ) for 30 min.  $\lambda_{\text{ex}} = 535$  nm,  $\lambda_{\text{em}} = 720$  nm.

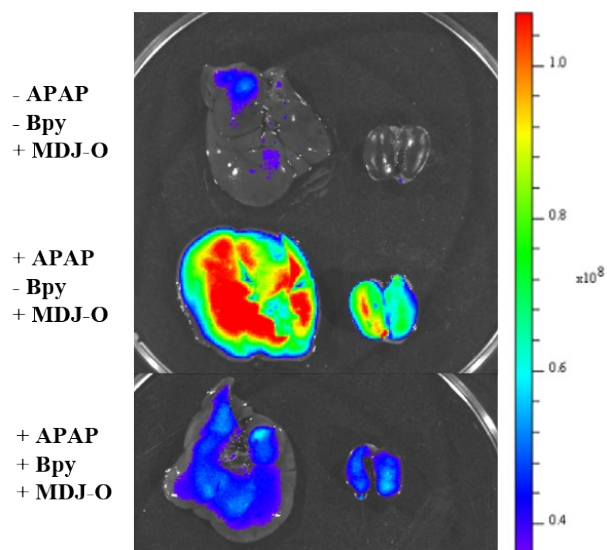


**Fig. S29.** Images of the livers and kidney ( $\lambda_{\text{ex}} = 535 \text{ nm}$ ,  $\lambda_{\text{em}} = 720 \text{ nm}$ ). From top to bottom: **MDJ-O** control group, APAP-induced group, and Bpy-treated group.

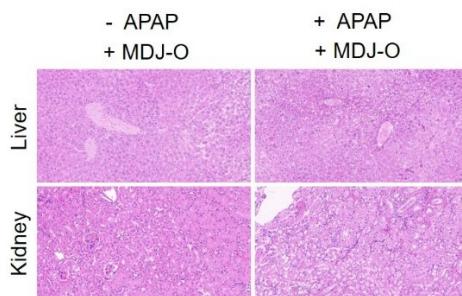


**Fig. S30.** H&E-stained liver and kidney sections of **MDJ-O** control group and APAP group ( $\times 20$  magnification).

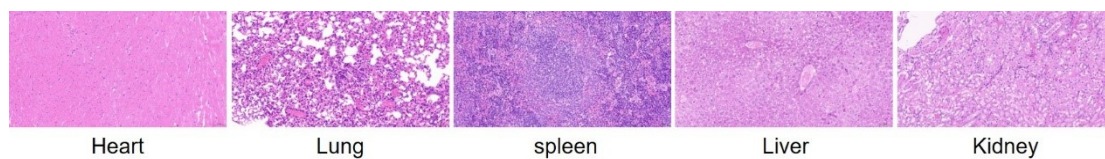


**Fig. S31.** H&E-stained internal organs sections of APAP group ( $\times 20$  magnification).

**Table S1.** Crystal data and structure refinement for **MDJ**.

---

Identification code	MDJ
Empirical formula	C <sub>25</sub> H <sub>27</sub> N <sub>3</sub>
Formula weight	369.49
Temperature/K	298.00
Crystal system	monoclinic
Space group	P2 <sub>1</sub> /c
a/Å	11.2287(4)
b/Å	11.3058(4)
c/Å	16.1029(6)
$\alpha$ /°	90
$\beta$ /°	100.4710(10)
$\gamma$ /°	90
Volume/Å <sup>3</sup>	2010.21(13)
Z	4
$\rho_{\text{calc}}/\text{cm}^3$	1.221
$\mu/\text{mm}^{-1}$	0.072
F(000)	792.0
Crystal size/mm <sup>3</sup>	0.2 × 0.04 × 0.02
Radiation	MoK $\alpha$ ( $\lambda$ = 0.71073)
2 $\Theta$ range for data collection/°	5.156 to 54.962
Index ranges	-14 ≤ h ≤ 14, -11 ≤ k ≤ 14, -20 ≤ l ≤ 19
Reflections collected	17350
Independent reflections	4484 [R <sub>int</sub> = 0.0358, R <sub>sigma</sub> = 0.0307]
Data/restraints/parameters	4484/0/255
Goodness-of-fit on F <sup>2</sup>	1.053
Final R indexes [I ≥ 2 $\sigma$ (I)]	R <sub>1</sub> = 0.0431, wR <sub>2</sub> = 0.1192
Final R indexes [all data]	R <sub>1</sub> = 0.0499, wR <sub>2</sub> = 0.1246
Largest diff. peak/hole / e Å <sup>-3</sup>	0.31/-0.17

---

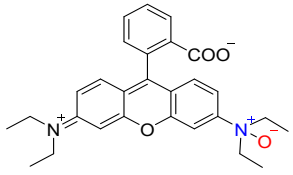
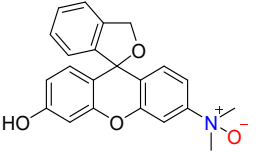
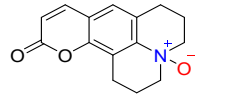
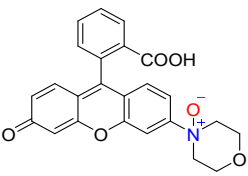
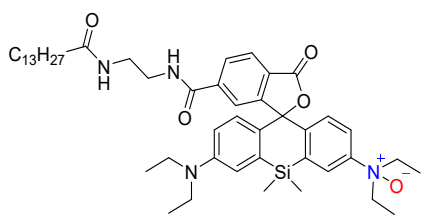
**Table S2.** Bond lengths [ $\text{\AA}$ ] for **MDJ**.

<b>Atom</b>	<b>Atom</b>	<b>Length/<math>\text{\AA}</math></b>	<b>Atom</b>	<b>Atom</b>	<b>Length/<math>\text{\AA}</math></b>
N3	C20	1.3690(13)	C10	C11	1.3688(15)
N3	C19	1.4592(14)	C10	C9	1.5075(15)
N3	C25	1.4578(14)	C11	C4	1.4274(14)
C14	C13	1.4463(14)	C9	C6	1.5367(14)
C14	C15	1.4017(14)	C4	C5	1.5021(16)
C14	C21	1.4083(14)	C4	C2	1.3786(15)
C13	C12	1.3558(15)	C5	C6	1.5352(14)
C15	C16	1.3816(14)	C3	C2	1.4321(17)
C21	C22	1.3786(14)	C2	C1	1.4341(15)
C20	C16	1.4207(14)	C6	C7	1.5265(16)
C20	C22	1.4220(14)	C6	C8	1.5301(16)
C16	C17	1.5102(14)	C23	C24	1.5204(16)
N1	C1	1.1487(16)	C19	C18	1.5085(16)
N2	C3	1.1483(17)	C25	C24	1.5109(16)
C12	C10	1.4384(14)	C17	C18	1.5183(16)
C22	C23	1.5075(14)			

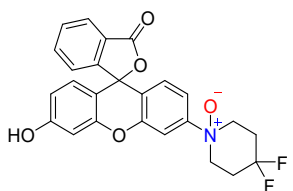
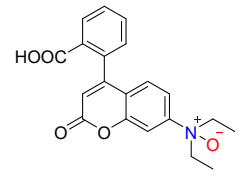
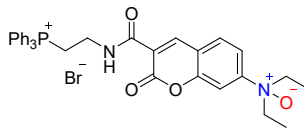
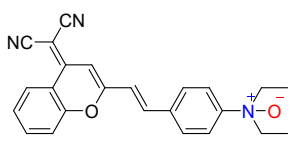
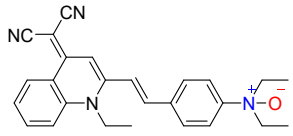
**Table S3.** Bond angles [°] for **MDJ**.

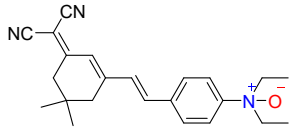
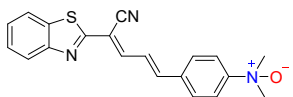
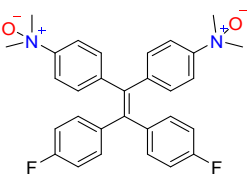
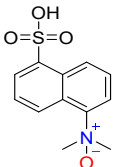
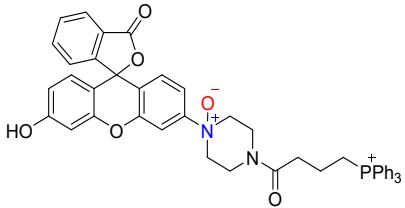
<b>Atom</b>	<b>Atom</b>	<b>Atom</b>	<b>Angle/°</b>	<b>Atom</b>	<b>Atom</b>	<b>Atom</b>	<b>Angle/°</b>
C20	N3	C19	122.19(9)	C10	C9	C6	113.92(9)
C20	N3	C25	122.80(9)	C11	C4	C5	118.17(10)
C25	N3	C19	114.82(9)	C2	C4	C11	121.66(10)
C15	C14	C13	119.68(10)	C2	C4	C5	120.15(10)
C15	C14	C21	116.74(9)	C4	C5	C6	112.80(9)
C21	C14	C13	123.57(9)	N2	C3	C2	178.10(14)
C12	C13	C14	127.33(10)	C4	C2	C3	122.38(10)
C16	C15	C14	123.00(10)	C4	C2	C1	121.63(11)
C22	C21	C14	122.50(9)	C3	C2	C1	115.99(10)
N3	C20	C16	120.88(9)	C5	C6	C9	108.09(9)
N3	C20	C22	120.29(9)	C7	C6	C9	110.03(9)
C16	C20	C22	118.83(9)	C7	C6	C5	110.89(9)
C15	C16	C20	119.22(9)	C7	C6	C8	109.30(10)
C15	C16	C17	121.61(10)	C8	C6	C9	109.56(9)
C20	C16	C17	119.16(9)	C8	C6	C5	108.95(9)
C13	C12	C10	125.58(10)	C22	C23	C24	110.04(9)
C21	C22	C20	119.65(9)	N3	C19	C18	112.18(9)
C21	C22	C23	121.75(9)	N1	C1	C2	179.13(13)
C20	C22	C23	118.60(9)	N3	C25	C24	112.83(9)
C12	C10	C9	120.23(9)	C25	C24	C23	109.63(10)
C11	C10	C12	119.91(10)	C16	C17	C18	110.33(9)
C11	C10	C9	119.86(9)	C19	C18	C17	110.42(10)
C10	C11	C4	122.98(10)				

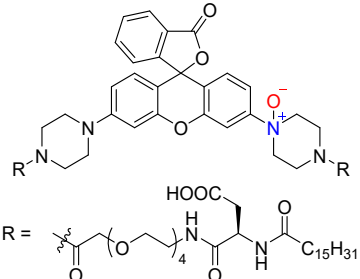
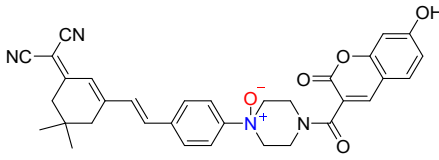
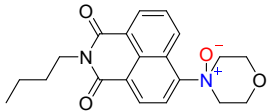
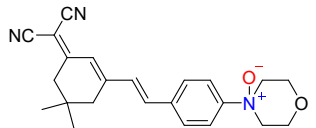
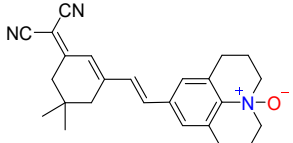
**Table S4.** Comparison of **MDJ-O** with other reported Fe<sup>2+</sup> probes containing *N*-oxide structure.

Sensors	Detection limit (M)	Ex/Em (nm)	Time response (min)	Solvent	Applications	Reference
	$2.0 \times 10^{-7}$	540/575	60	HEPES buffer	HepG2 cells	[1] Chem. Sci 2013, 4, 1250.
	—	515/535	60	HEPES buffer (0.2% DMF)	HepG2 cells	[2] Org. Biomol. Chem 2014, 12, 6590.
	—	295/495	30	HEPES buffer	HepG2 cells	[3] Chem. Sci 2017, 8, 4858.
	—	450/530	50	HEPES buffer	HepG2 cells	[3] Chem. Sci 2017, 8, 4858.
	$5.0 \times 10^{-8}$	630/665	30	HEPES buffer (30% dioxane)	HepG2 cells	[4] Chem. Sci 2019, 10, 1514



	—	490/535	30	HEPES buffer (0.2% DMSO)	HeLa cells	[5] J. Am. Chem. Soc 2022, 144, 3793.
	$7.6 \times 10^{-8}$	400/515	—	HEPES buffer (5% DMSO)	—	[6] ACS Appl. Bio. Mater 2020, 3, 4074.
	$2.0 \times 10^{-6}$	390/460	60	HEPES buffer (0.2% DMSO)	HeLa cells	[7] J. Photochem. Photobiol. B 2020, 209, 111943.
	$4.5 \times 10^{-6}$	540/690	15	PBS buffer (50% DMSO)	MCF-7 cells	[8] Sens. Actuators B 2019, 288, 217.
	$4.2 \times 10^{-7}$	480/630	5	Sodium borate buffer	HepG2 cells	[9] Dyes Pigm 2021, 190, 109271.

	$2.7 \times 10^{-8}$	400/675	5	PBS buffer (40% DMSO)	HepG2 cells; Zebrafish	[10] J. Hazard. Mater 2021, 406, 124767.
	$2.1 \times 10^{-7}$	467/625	20	PBS buffer (30% EtOH)	RAW 264.7 macrophage cells; Zebrafish	[11] J. Lumin 2022, 250, 119069.
	—	360/515	10	PBS buffer	HeLa cells	[12] Adv. Funct. Mater 2019, 29, 1903278.
	$1.8 \times 10^{-8}$	350/489	20	Tris buffer (20% DMSO)	Kyse180 cells	[13] Talanta 2020, 215, 120908.
	$1.0 \times 10^{-6}$	540/575	60	HEPES buffer (0.2% DMSO)	HepG2 cells	[14] ACS Sens 2020, 5, 2950.

	—	540/575	60	HEPES buffer (0.2% DMSO)	HepG2 cells	[15] ACS Chem. Biol 2018, 13, 1853.
	$7.5 \times 10^{-8}$	430/675	30	Tris-HCl buffer (30% DMSO)	A549 cells; Kunming mice	[16] Sens. Actuators B 2022, 371, 132512.
	$1.02 \times 10^{-6}$	395/540	30	Aqueous solution (0.5% CH <sub>3</sub> CN)	—	[17] Chem. Commun 2019, 55, 12136.
	$1.42 \times 10^{-8}$	456/640	10	PBS buffer (1% DMSO, 1 mM CTAB)	Neuronal cells; Balb/c mice	[18] Cell Chem. Biol 2022, 29, 43.
	$3.09 \times 10^{-6}$	540/720	5	PBS buffer (2.5% EtOH, 1 mM CTAB)	HepG2 cells; Zebrafish; Kunming mice	This work

## References:

1. T. Hirayama, K. Okuda, H. Nagasawa. *Chem. Sci.*, 2013, **4**, 1250–1256.
2. M. Niwa, T. Hirayama, K. Okuda, H. Nagasawa, *Org. Biomol. Chem.*, 2014, **12**, 6590–6597.
3. T. Hirayama, H. Tsuboi, M. Niwa, A. Miki, S. Kadota, Y. Ikeshita, K. Okuda, H. Nagasawa, *Chem. Sci.*, 2017, **8**, 4858–4866.
4. T. Hirayama, M. Inden, H. Tsuboi, M. Niwa, Y. Uchida, Naka Y, I. Hozumib, H. Nagasawa, *Chem. Sci.*, 2019, **10**, 1514.
5. K. Kawai, T. Hirayama, H. Imai, T. Murakami, M. Inden, I. Hozumi, H. Nagasawa, *J. Am. Chem. Soc.*, 2022, **144**, 3793–3803.
6. E. Ahmmed, A. Mondal, A. Sarkar, S. Chakraborty, S. Lohar, N.C. Saha, K. Dhara, P. Chattopadhyay, *ACS Appl. Bio. Mater.*, 2020, **3**, 4074–4080.
7. S. Khatun, S. Biswas, A. Binoy, A. Podder, N. Mishra, S. Bhuniya, *J. Photochem. Photobiol. B*, 2020, **209**, 111943.
8. X. Yang, Y. Wang, R. Liu, Y. Zhang, J. Tang, E. Yang, D. Zhang, Y. Zhao, Y. Ye, *Sens. Actuators B Chem.*, 2019, **288**, 217–224.
9. L. Yang, Q. Chen, S. Gan, Q. Guo, J. Zhang, H. Zhang, Y. Xie, H. Xiao, W. Wang, H. Sun, *Dyes Pigm.*, 2021, **190**, 109271.
10. M. Zhu, Z. Zhao, X. Liu, P. Chen, F. Fan, X. Wu, R. Hua, Y. Wang, *J. Hazard. Mater.*, 2021, **406**, 124767.
11. X. Zeng, J. Chen, S. Yu, Z. Liu, M. Ma, *J. Lumin.*, 2022, **250**, 119069.
12. C. Xu, H. Zou, Z. Zhao, P. Zhang, R. T. K. Kwok, J. W. Y. Lam, H. H. Y. Sung, I. D. Williams, B. Z. Tang, *Adv. Funct. Mater.*, 2019, **29**, 1903278.
13. G. Ga, X. Wang, Z. Wang, X. Jin, L. Ou, J. Zhou, P. Xie, *Talanta*, 2020, **215**, 120908.
14. T. Hirayama, M. Niwa, S. Hirosawa, H. Nagasawa, *ACS Sens.*, 2020, **5**, 2950–2958.
15. M. Niwa, T. Hirayama, I. Oomoto, D.O. Wang, H. Nagasawa, *ACS Chem. Biol.*, 2018, **13**, 1853–1861.
16. S. Feng, J. Zheng, J. Zhang, Z. Gui, G. Feng, *Sens. Actuators B Chem.*, 2022, **371**, 132512.
17. Y.H. Lee, P. Verwilst, H.S. Kim, J. Ju, J. S. Kim, K. Kim, *Chem. Commun.*, 2019, **55**, 12136–12139.
18. C. Shao, Y. Liu, Z. Chen, Y. Qin, X. Wang, X. Wang, C. Yan, H. Zhu, J. Zhao, Y. Qian, *Cell*

*Chem. Biol.*, 2022, **29**, 43–56.